applied sciences

MDPI

Article

A Stability Analysis of an Abandoned Gypsum Mine Based on Numerical Simulation Using the Itasca Model for Advanced Strain Softening Constitutive Model

Yungang Shi [1], Huaijian Wang [2], Xin Tan [3,*], Yuxuan Jin [1], Jiaxu Wang [3] and Bigang Tang [1]

1 Hunan Communications Research Institute Co., Ltd., Changsha 410015, China; shiyungang1217@163.com (Y.S.); yuxuanjin973@gmail.com (Y.J.)
2 CCCC Construction Group Co., Ltd., Beijing 100022, China
3 College of Civil Engineering, Hunan University, Changsha 410082, China
* Correspondence: xintan@hnu.edu.cn; Tel.: +86-15580373653

Abstract: An abandoned gypsum mine has been discovered beneath the route of a highway construction in Hunan province, south China. Due to the highway construction and operations safety, there is an urgent need for a comprehensive stability analysis of the abandoned mining area. The 3D laser scanning detection technique has been adopted, and over 400 drillholes were strategically placed near the highway to capture the spatial information of the abandoned gypsum mine. The ore body has an average mining thickness of about 3 m, and the depth of the mining roof ranges from 40 to 60 m, with an average span of 16 m. Based on the research achievements in the engineering geological investigation, rock mass quality assessment, and geometry information, a simplified numerical model has been established for stability analysis. The numerical model employed the IMASS rock mass constitutive model to conduct a stability analysis of the abandoned gypsum mine during the excavation process and in the medium to long term. The IMASS constitutive model can effectively reflect the entire process of rock mass from microscopic damage to macroscopic instability, and the numerical simulation of current and long-term stages provides a much greater understanding of the mining room stability and the effect of various geo-mechanical parameters not considered in traditional empirical methods. The abandoned gypsum mine stability is guaranteed in the mining and current stages. However, the numerical results showed that a 0.4 m spalling thickness of the sidewalls can cause an overall instability and failure of the abandoned mine, and reinforcement measures must be taken for long-term safety. The stability of the abandoned gypsum mine with filling solutions was also evaluated numerically.

Keywords: gypsum mine; stability analysis; laser scanning; goaf; numerical simulation

check for updates

Citation: Shi, Y.; Wang, H.; Tan, X.; Jin, Y.; Wang, J.; Tang, B. A Stability Analysis of an Abandoned Gypsum Mine Based on Numerical Simulation Using the Itasca Model for Advanced Strain Softening Constitutive Model. *Appl. Sci.* **2023**, *13*, 12570. https://doi.org/10.3390/app132312570

Academic Editor: Tiago Miranda

Received: 11 September 2023
Revised: 31 October 2023
Accepted: 2 November 2023
Published: 22 November 2023

1. Introduction

Gypsum, as an important mineral resource, plays a significant role in socio-economic development. In the southern regions of China, due to unregulated mining of private gypsum mines, numerous unknown goaf areas have been created, posing potential hazards to subsequent transportation infrastructure construction and operational safety. Gypsum is a soluble mineral, especially in environments with groundwater, making it prone to dissolution [1]. Therefore, the stability of abandoned gypsum mine areas can easily be influenced by groundwater, potentially leading to the dissolution and damage of the mineral body. Room-and-pillar mining is a commonly used method for gypsum mining, where mined-out pillars or sidewalls are left underground for an extended period. Under the long-term effects of overlying rock loads and groundwater infiltration, these supports can sustain damage and deterioration. Many gypsum mine pillars become unstable due to prolonged damage beyond their limits, resulting in extensive collapse disasters [2–4].

The stability issues of abandoned gypsum mine areas have garnered increasing attention. Yang et al. (2015) [5] highlighted several serious accidents caused by collapses in abandoned gypsum mines. Studies on various engineering cases have indicated that proper assessment and treatment measures can effectively ensure the stability of gypsum mines, reducing the occurrence of geological disasters. Therefore, conducting research on the stability and instability mechanisms of gypsum mine goaf areas holds significant importance [6,7]. The assessment of gypsum mine goaf area stability involves various tasks, such as rock mechanics tests, geological structure investigations, and stress field analysis. Through field investigations and laboratory tests, the mechanical parameters of the gypsum rock mass, as well as the geological structures and stress field distributions, are determined in order to assess the stability of the goaf area.

Henley et al. (1976) [8] employed an energy theory to analyze the dynamic process of instability in gypsum mine systems. Auvray et al. (2004, 2008) [9,10] used SEM (scanning electron microscope) to observe the weathering process of gypsum mine pillars in abandoned mine areas. The results showed that the weathering rate of gypsum mine pillars is related to the duration of mining activities. The time-related characteristics of gypsum mine pillars are closely linked to the air humidity inside the abandoned mine area, which is influenced by ventilation conditions and seasonal variations. Zhao et al. (2010) [11] applied a catastrophe theory in combination with the safety factor reduction method to evaluate the stability of abandoned mine roofs.

Numerical simulation methods have been widely applied in the stability assessment of gypsum mine areas. By establishing numerical models, these methods simulate mining processes such as stress distribution, displacement, deformation, and fracture within the gypsum mine, predicting its stability and optimizing remediation measures. Pierce and Cundall (2004) [12] simulated surface subsidence caused by block caving mining using the discontinuous fracture model and particle flow algorithm. Their research provided important numerical simulation methods for understanding and predicting ground subsidence mechanisms due to mining activities. Cai et al. (2007) [13] proposed a new method based on the GSI (Geological Strength Index) system, obtaining relevant parameters of jointed rock masses through field investigations and experimental measurements for numerical simulation and engineering design. This method is significant for assessing the stability of jointed hard rock and designing underground mining projects. Alejano [14] and Gomez (2013) developed a stability assessment method for blocky rock mass caverns by combining field observations and numerical simulations, which considered fracture characteristics and stress distribution in the rock mass, enabling a more accurate evaluation of the stability in such rock mass caverns. Fidelibus [15] and Soccodato (2002) simulated stress and displacement distributions during the underground limestone mining process in the Apulia region of Italy, studying stability and collapse mechanisms during mining activities. Zou and Konietzky (2016) [16] simulated the inflow of karst water during underground mining activities, analyzing the interaction between groundwater and mining operations.

In 2009, the local government temporarily closed the mining operation of this gypsum mine. However, due to financial difficulties, no investigation or proper disposal of the abandoned mining area took place after the mine closure. Until now, only one inclined shaft was left operational for water pumping maintenance. Consequently, there is a severe lack of reliable preliminary data concerning this abandoned mining area, resulting in a complete lack of knowledge regarding the conditions of the drifts and stope rooms. This lack of information presents significant challenges for conducting a stability analysis and implementing engineering solutions for the abandoned mining area.

Based on the research achievements in the engineering geological investigation, rock mass quality assessment, and geometry model construction, this study considered the current and long-term state of an actual abandoned gypsum mine in south China. It utilized numerical methods and employed the IMASS (Itasca Model for Advanced Strain Softening) constitutive model to conduct a stability analysis of the abandoned gypsum mine in terms of its current and long-term state.

2. Engineering Background

2.1. Engineering Geology

During the engineering geological survey for the Baiguo-Nanyue highway construction in Hunan province, China, an abandoned gypsum mine was discovered beneath the route (Figure 1). Considering that there is a proposed bridge above this abandoned mining area, and that the gypsum rock is highly soluble in water, the potential for extensive pillar or roof collapse in this area is significant, which could undoubtedly lead to a serious geologic hazard. Therefore, in accordance with relevant construction standards, this section of the highway was designated as an unstable site, necessitating a more comprehensive investigation and stability analysis.

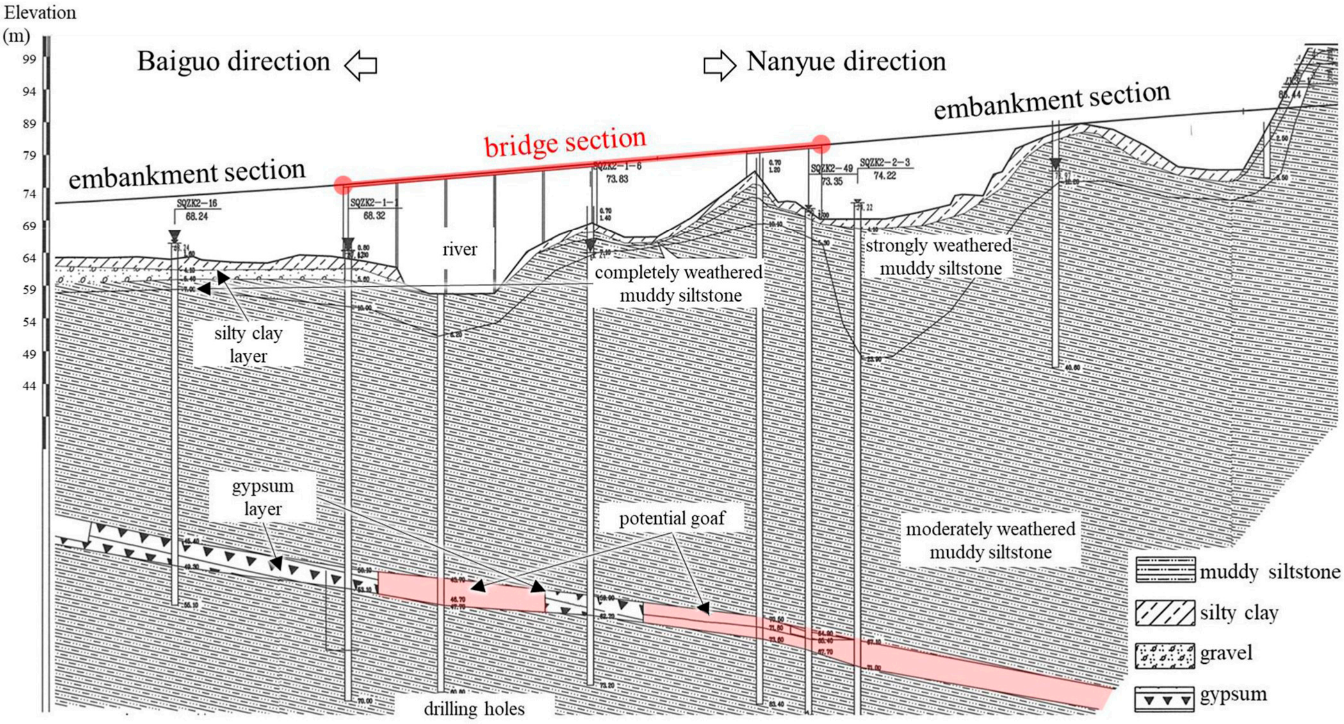

Figure 1. Engineering geology overview.

The topography above the abandoned mining area is characterized by an alluvial plain with a relatively simple terrain, where the maximum altitude difference is approximately 3.0 m. Based on the report of the geological survey from boreholes, the stratum in this area predominantly consists of Quaternary Holocene sedimentary layers, including fill, silty clay, fine sand, and gravelly soil; the bedrock is composed of Cretaceous argillaceous siltstone; and below 10 to 20 m burial depth is a layer of medium-weathered argillaceous sandstone with a silty fine-grained structure and medium-thick layered arrangement, and joint cracks are generally slightly developed. Notably, this layer contains a 1.5 to 4.0 m thick stratum of green gypsum. The geological structure of this area lacks extensive development, and the underlying bedrock follows a monoclinal structure with a nearly horizontal bedding orientation. The geophysical exploration and borehole data indicate that the goaf's burial depth beneath the highway central line is between 30 and 80 m, with the goaf's height measuring around 3 m.

2.2. 3D Laser Scanning and Detection Results

Traditionally, the assessment methods for abandoned mining areas include geological drilling, geophysical prospecting, 3D laser scanning detection, and similar techniques. Among these methods, 3D laser scanning technology is particularly valuable, as it accurately captures spatial information in the form of point clouds at the area's boundaries.

Furthermore, this technology enables the generation of precise 3D models through specialized point cloud processing programs.

The project utilizes the HVM100 SLAM 3D laser scanning system, which is a continuous scanner with SLAM technology developed by the Commonwealth Scientific and Industrial Research Organisation (CSIRO) of Australia. It utilizes laser ranging to acquire information about the surrounding environment. The data acquisition speed is 300,000 points per second, with a weight of only 1.8 kg. It has a distance accuracy of ±4 cm, an angular resolution of 0.1°, and a measurement range of 360° × 360° with no blind spots.

The highway construction company undertook 3D laser scanning detection for the abandoned mining area. The detection process is depicted in Figure 2: A laser scanner was inserted into the abandoned mining area through a drillhole; the scanner, capable of a 360-degree rotation, continuously collected data on the distances and angles of the measured points during the detection process; data accuracy was meticulously maintained by controlling three parameters, including the scanning center's coordinates, the scanning angle, and the measuring distance. In total, over 400 drillholes were strategically placed near the highway, and the data collection for all drillholes was successfully carried out using a 3D laser detection system.

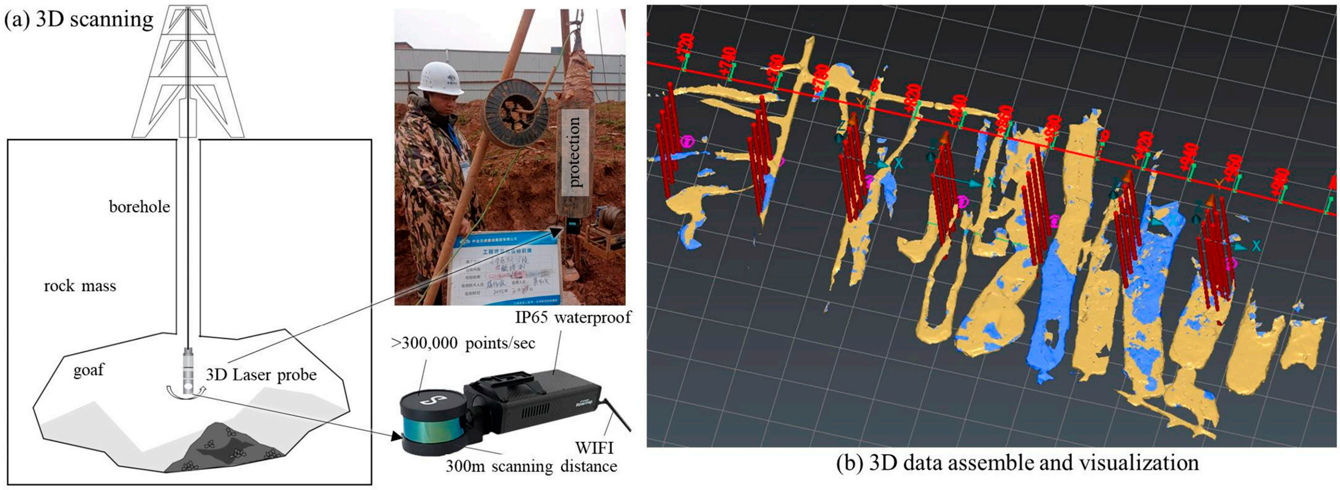

Figure 2. 3D laser scanning detection and results.

The 3D point cloud data collected from these drillholes were processed through a dedicated 3D point cloud data processing system, leading to the reconstruction of a 3D spatial model for the abandoned mining area, as illustrated in Figure 2b. This approach facilitates the automatic calculation of the roof area and the volume of the abandoned mining area.

2.3. Engineering Impact and Status Evaluation

Based on the findings from the 3D laser detection, Figure 3 illustrates the plan view of the abandoned mining area adjacent to the highway bridge foundations. The mining method employed here was room-and-pillar mining, a technique involving the excavation of "rooms" into the rock mass while leaving behind "pillars" of unexcavated material to support the roof. This creates a grid-like pattern of extracted areas and supporting structures, balancing the need for resource extraction with maintaining the stability of the surrounding environment. The primary mine shaft runs in a north–south direction. The ore body is present as stratoid beds with an average mining thickness of around 3 m. In this specific case of room-and-pillar mining, the pillars and remaining structures were not sufficiently robust to prevent some level of collapse and instability, which is indicative of the challenges and considerations that come with this mining method. Among the mining rooms, only a few have been backfilled with waste slag, while the majority remain unfilled, lacking significant lateral constraints. The exposed area of the abandoned region, near the bridge foundation, is extensive, accounting for roughly 84% of the total ore body area. The mining rooms are predominantly elongated, with their orientation approximately orthogonal to the highway central line. The maximum length of the mining room is about 150 m, which is much longer than the room width. The roof depth varies between 40 and 60 m, and the mining rooms span from 14 to 24 m, with an average span of 16 m, maintaining an equal width on both sides. It is worth noting that the average width of the side walls and pillars is only 3 m, and many pillars were severely overmined, and some even collapsed. This highlights another aspect of room-and-pillar mining, where the size and integrity of the pillars are crucial to the long-term stability of the mined areas. There is a recurring pattern of interconnected mining rooms, and a significant portion of these rooms exhibit signs of roof collapse, underscoring the importance of carefully planned and executed room-and-pillar mining to mitigate such risks.

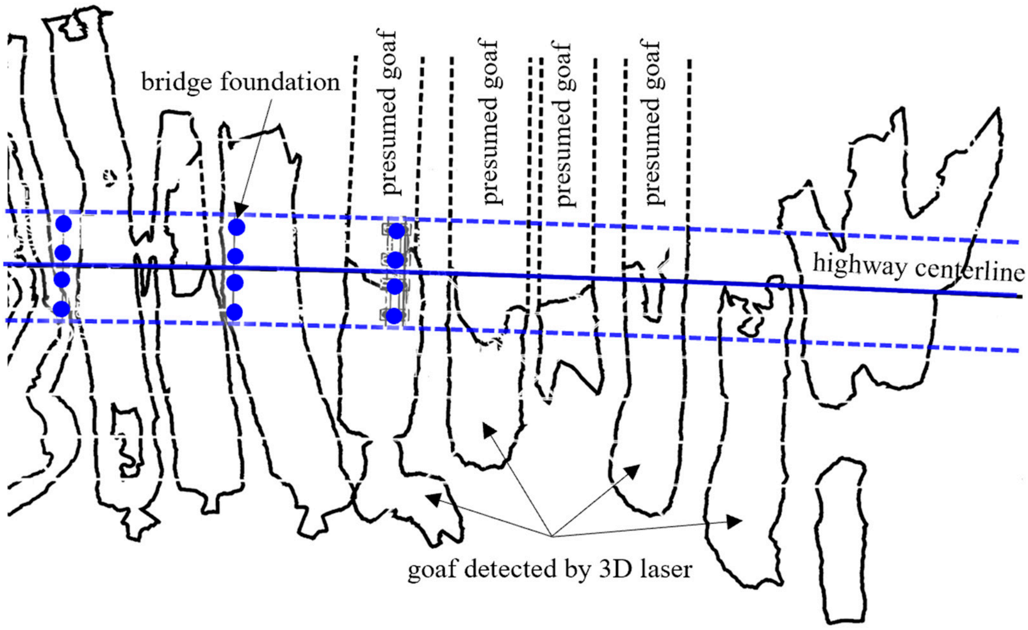

Figure 3. Plan view of the abandoned mining area.

The detection results indicate that several pillars within the mining area have already experienced subsidence. Moreover, the volume and extent of the abandoned mining area raise concerns. Consequently, the stability of the supporting system becomes increasingly challenging, especially in the face of long-term pressure transfer and water-induced softening. The enduring stability of the abandoned mining area is primarily contingent upon the stability of the roof and the rib. When the exposed areas of the roof and rib become extensive, instability becomes almost certain. Under these circumstances, there is an urgent need to conduct a comprehensive stability analysis of the abandoned mining area. This analysis is vital to ensuring the highway's safety and averting potential catastrophic accidents.

According to the results of the geological survey and 3D laser detection, although the gypsum mine has left roof pillars during the mining process, due to the large volume of the empty area, some of the pillars have already collapsed. It will be difficult to maintain the stability of the pillars under the influence of long-term stratum pressure transfer and softening of the water seepage. The long-term stability of the mining area will be mainly controlled by the stability of the roof and sidewalls. When the exposed area of the roof plate and sidewalls of the mining area is too large, the roof plate and sidewalls will be destabilized, which may result in the room collapsing, or even in large subsidence. In order to ensure the safety of the upper highway construction and prevent catastrophic accidents induced by the destabilization of the mining area, it is urgent to analyze the stability of the abandoned mining area.

3. Numerical Modeling

3.1. IMASS Constitutive Model

The brittle failure characteristics of rock mass, which exhibit material-softening and -bulking behaviors, are essentially important for modeling the rock damage around an underground excavation. A new constitutive model named the IMASS model (Itasca Model for Advanced Strain Softening model [14]) has been developed by Ghazvinian et al. (2020) to consider the progressive failure of the rock mass. It is able to represent the damage around an excavation, slope, or caving process where we must account for the progressive failure and disintegration of the rock mass from an intact/jointed condition to a bulked material. The conceptual model has been introduced by Duplancic and Brady (1999) [15] based on four main behavior zones, as shown in Figure 4a. An elastic zone means undisturbed rock mass; a seismogenic zone may generate microseismic activity due to discontinuity damage; a yielded zone is subject to significant damage, is fractured, and has lost most of its cohesion and provides minimal support to the excavation; and a mobilized zone gives an estimate as to the portion of the collapsed rock mass.

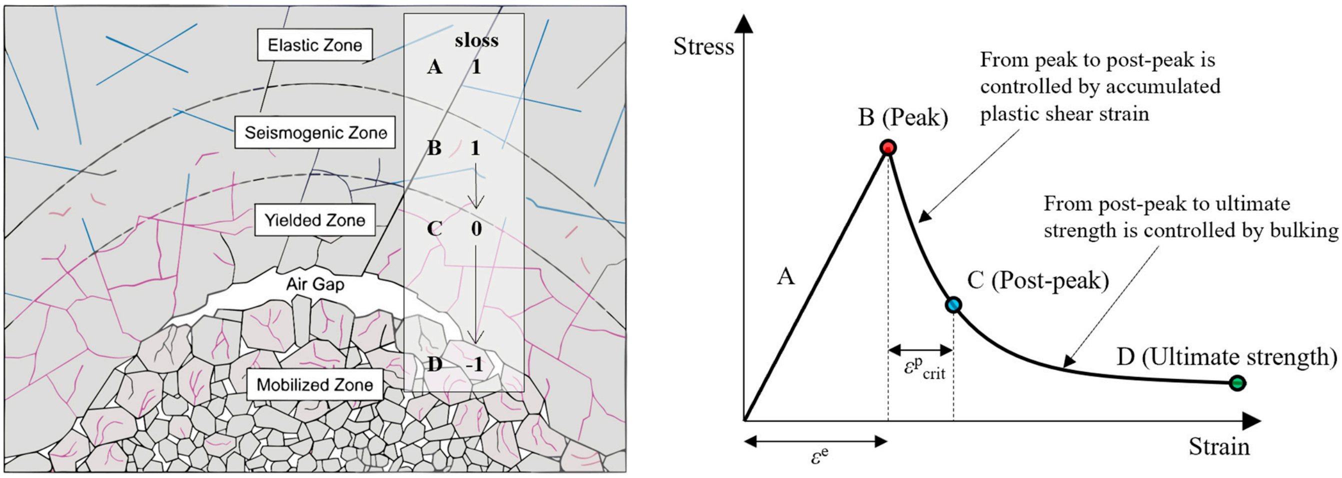

(**a**) (**b**)

Figure 4. IMASS schematic diagram: (**a**) Schematic representation of sloss for various degrees of damage in a rock mass (modified from Ghazvinian et al., 2020 [17]); (**b**) material response in the IMASS constitutive model.

Regarding groundwater in this region, it consists of pore water within the loose collapsed mass layer and fissured water within the bedrock. The pore water primarily exists within the Quaternary loose collapsed mass layer, sourced from atmospheric precipitation and surface water runoff. The groundwater volume contained within the pores is relatively small and exhibits seasonal variation. The average permeability coefficient of the medium-weathered argillaceous siltstone is calculated to be 0.0512 m/day, classifying it as a slightly permeable layer.

The peak behavior of the IMASS model is grounded in the Hoek–Brown [18,19] constitutive model. The intricate process of rock strain softening induces strain-dependent material characteristics within the damaged rock, as illustrated in Figure 4b. The IMASS constitutive model has been developed to simulate the response of such rock properties to changes in stress. The model employs an indicator termed “Sloss” to quantify the extent of softening or weakening experienced by a rock mass, with its range being [−1, 1].

Between peak and post-peak points in Figure 4b,

$$\text{Sloss} = 1 - \frac{\text{plastic shear strain}}{\text{critical plastic shear strain}}$$

Between post-peak and ultimate strength points,

$$\text{Sloss} = -\frac{\text{volumetric strain}}{\text{maximum allowable volumetric strain}}$$

Figure 4 schematically portrays the sloss parameter across various degrees of damage and disturbance within a rock mass. At point "C", the rock mass is assumed to have fractured, yet the resulting rock fragments remain fully interlocked (with cohesion fully lost but high friction). At this stage, the stress surpasses the spalling or fracturing strength of the rock. In contrast, at point "D", the interlocking of rock fragments is minimized, resulting in maximized porosity. Excavations that lack support within this stress state are deemed unstable.

3.2. Parameters and Numerical Model Setup

This section employed FLAC3D, a finite-difference-based method, to construct a numerical model for simulating the gypsum mining room excavation. Due to the excessive scope of the gypsum mining area, it is difficult to build a complete large-scale numerical model for the stability analysis, but since the mining area has symmetrical mine rooms, the model was simplified as depicted in Figure 5. It has overall dimensions of 10 m in width and 73 m in height. Given the typical ground conditions of the abandoned mining area, the maximum length of the mining room is about 150 m, which is much longer than the room width, and the model was designed as a planar strain model. The model's bottom and sides were subjected to simple support constraints, while the top was treated as a free boundary. Due to the symmetric nature of one mining room, the simplified numerical model included a mining room sidewall of 3 m $\times$ 3 m and a mining room of 17 m $\times$ 3 m. Only the medium-weathered rock layer and pre-existing gypsum rock layer were incorporated into the numerical model, as the gravel and strongly weathered rock layers were confined to the shallow layers of the ground and did not significantly impact the abandoned mining area's stability.

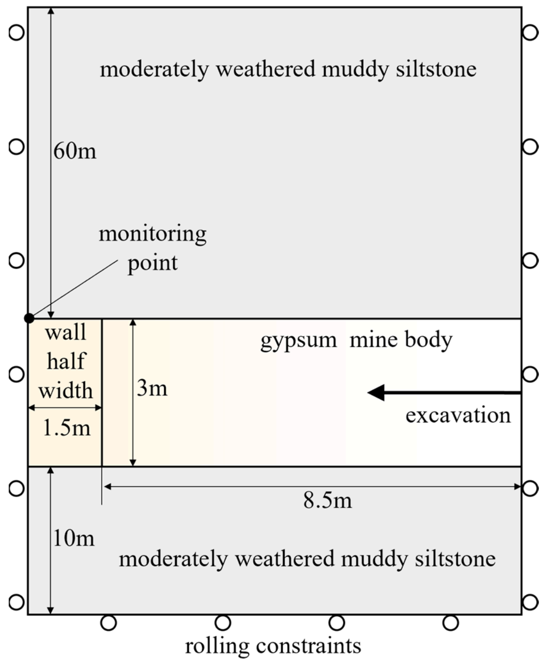

Figure 5. Numerical model setup for current stability.

The mining process inevitably disrupts the initial stress equilibrium within the original rock mass, leading to a redistribution of stress. As stress is rebalanced, the weight of the rock mass above the mining room shifts to the stable adjacent regions, resulting in a stress concentration along the residual sidewalls. Under the assumption of considering only the self-weight load, the failure of the abandoned mining area is expected to initiate from the sidewalls when the stress exceeds the rock mass's strength limit. To track this, a monitoring point has been established at the top of the sidewall to record vertical stress and displacement, as shown in Figure 5.

The GSI, mi, and UCS parameters play a crucial role in shaping the peak Hoek–Brown envelope, and these relationships are defined through the equations established by Hoek et al. (2002). A significant element of the IMASS model is the residual envelopes and the phenomenon of rock mass softening that occurs after reaching the peak envelope. This phenomenon is extensively elaborated upon in the introduction of "cohesion weakening frictional Strengthening behavior [20]". The properties listed in Table 1 represent the essential input properties necessary for the implementation of the IMASS constitutive model. These properties were carefully selected based on geological survey data to ensure the model's accuracy and reliability.

Table 1. Numerical model parameters for goaf.

	Density	Geological Strength Index (GSI)	Hoek–Brown Parameter mi	Uniaxial Compressive Strength	Elastic Modulus	Multiplier Factor
	kg/m^3	/	/	MPa	GPa	
Gypsum ore	2400	75	15	25	8	0.1
Moderately weathered muddy siltstone	2475	65	10	50	10	0.5

The critical plastic shear strain for the IMASS model, as indicated in Table 1, employs a multiplier to compute the critical strain, as visually demonstrated in Figure 1. By adjusting this multiplier, the material behavior can be modified to exhibit increased brittleness if the multiplier is set to a value less than 1.0, or heightened ductility if its value is set to be greater than 1.0. This multiplier factor serves to adjust the post-peak mechanical properties of rocks, as rock mass undergoes progressive damage during the loading process. After failure, the rock mass does not completely lose its bearing capacity under certain stress conditions. Therefore, the post-peak mechanical behavior still influences the overall bearing capacity of the model. Specifically, this is manifested by the speed at which the stress–strain curve drops to its residual strength after the peak strength, representing brittleness and plasticity.

4. Numerical Analysis

4.1. The Excavation Process and Current Stability Analysis

The excavation process of the numerical model commenced on the right side of the mining room. The excavation procedure required periodic suspensions at every 2 m length interval to allow the stress in the surrounding rock mass to achieve equilibrium. Figure 6 provides an insight into the vertical stress and displacement at the top of the sidewall throughout the excavation, while Figure 7 presents the vertical stress distribution in the surrounding rock mass during various excavation stages.

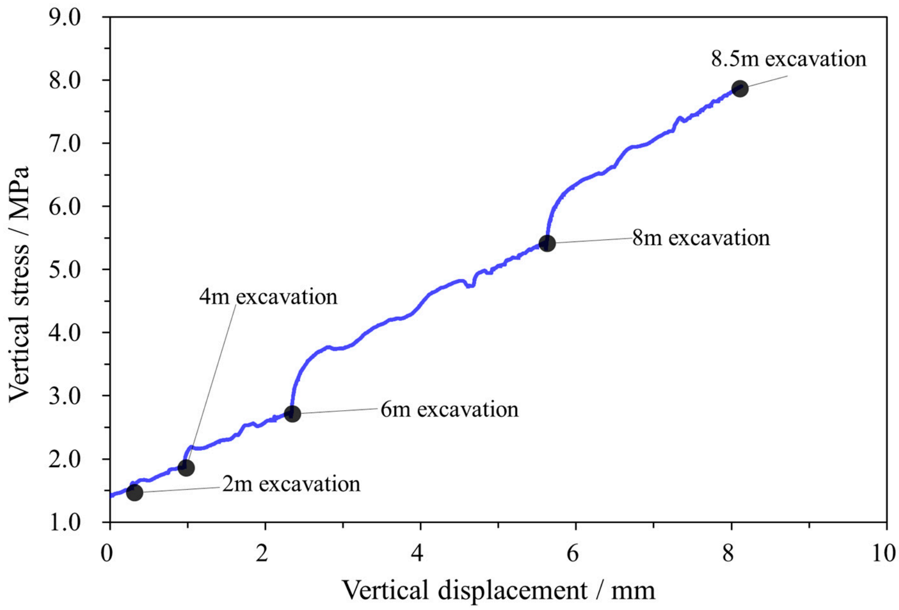

Figure 6. Vertical stress–vertical displacement curve at the monitoring point of current stability.

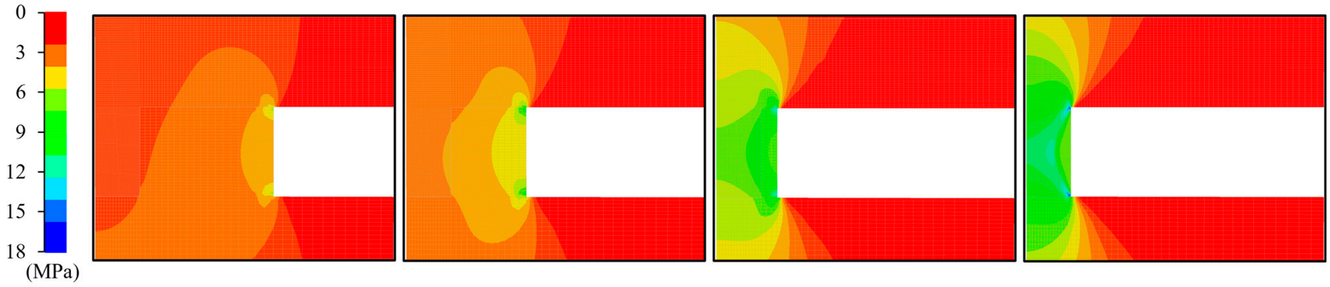

(**a**) 4 m (**b**) 6 m (**c**) 8 m (**d**) 8.5 m

Figure 7. Vertical stress evolvement at different excavation states.

Evidently, when the excavation face maintained a considerable distance from the sidewall, only minor disturbances were observed. The vertical stress at the monitoring point altered from 1.5 MPa to 2.5 MPa as the excavation length reached 6 m. However, as the thickness of the sidewall diminished, the increment in stress escalated rapidly. For instance, when the excavation depth reached 8 m, the vertical stress surged to 5.5 MPa. The analysis of the stress distribution illustrated that the vertical stress at the monitoring point exhibited intermediate levels within the overall stress distribution of the sidewall.

Furthermore, the phenomenon of stress concentration stemming from the excavation emerged initially at the corner of the sidewall and subsequently propagated towards the central region. Upon the completion of the excavation, the vertical stress in the central region reached 10 MPa, yet it could peak at 18 MPa in the corner. This occurrence indicates that the stress on the sidewall during the excavation process could closely approach the uniaxial compressive strength of gypsum rock in a laboratory (25 MPa). The stress concentration might lead to localized rock damage at the corners and free surface. Nonetheless, the general stability of the sidewall in the current stage remains assured.

Figure 8 illustrates the progression of the plastic state of the surrounding rock mass at various excavation stages. Following the completion of excavation, the rock roof of the abandoned mining area lost its support, leading it to bend downward under the pressure exerted by the overlying rock. Due to the relatively weak tensile strength of the rock, elements within a certain thickness of the roof underwent tension failure as the stress surpassed the tensile strength limit. As the excavation concluded, the failed elements within the roof connected with each other, forming a rupture surface. Consequently, a roof collapse occurred, resulting in a nearly 1 m thick fallen region at the mining room top. Contrasted with its tensile strength, gypsum's compressive strength is notably stronger. Hence, it was not until the excavation length reached 8 m that the sidewall began to yield (Figure 8c). Upon the completion of the excavation, both sides of the side wall gave rise to a shear zone Figure 8d). The stress within the shear zone of the gypsum rock did not exceed its yield strength, adhering to the principles of elasticity. This region was enveloped and confined by the yield zone, experiencing a three-directional stress state. This region can be aptly termed the elastic core region of the sidewall.

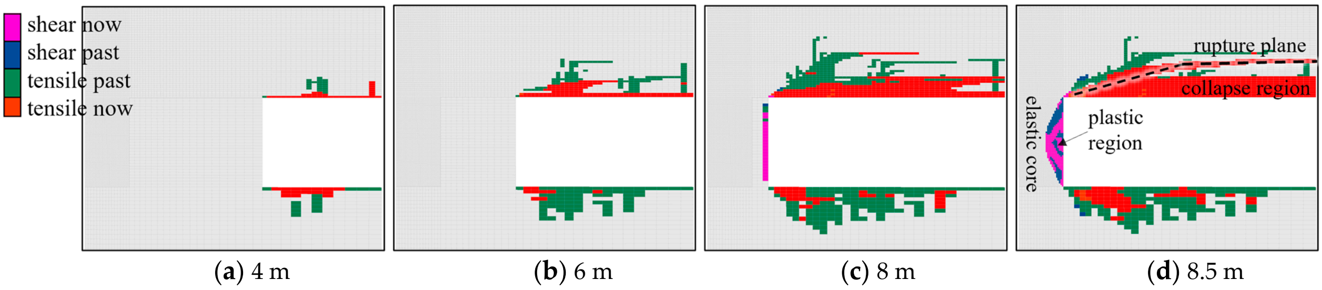

Figure 8. Plastic region evolvement at different excavation states.

In Figure 8, "shear now" indicates that elements have entered shear failure during the current calculation step, while "tensile now" suggests that elements are currently experiencing tensile failure during the respective calculation step. "shear past" indicates a previous state of shear failure. "tensile past" denotes a previous state of tensile failure.

Compared with the plastic state, the IMASS model's sloss indicator more accurately reflects the failure process of the brittle rock mass. Figure 9 presents the distribution of the sloss index at the final excavation state. On both sides of the remaining sidewall, a region with sloss index values ranging from 0.95 to 1.0 was observed. This indicated that the stress within this zone had just exceeded the peak strength and had entered the stage of strength degradation. As the strength of the elastic core was still sufficient to bear the transferred stress from excavated room, the strength degradation did not escalate rapidly. Consequently, the sloss index remained slightly below 1.0.

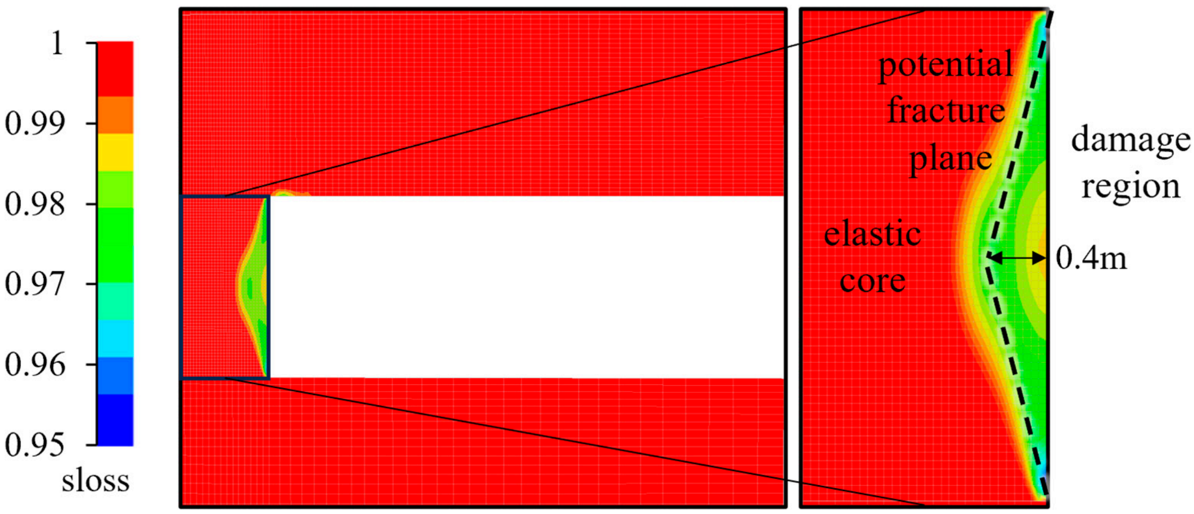

Figure 9. Rock damage conditions (sloss index) at final excavation state.

The regions characterized by low sloss index values can be perceived as potential rupture surfaces. The stress within these regions was very close to or even surpassed the rock's peak strength. While they might not experience immediate destruction, there is a high likelihood of further damage, rupture, and spalling failure from the sidewall to the empty room over the medium to long term. The rock mass within the potential rupture surface of the sidewall is referred to as the elastic core region, which is distributed in a "vertical barbell" form. This elastic core plays a pivotal role in bearing the overburden pressure over the long term.

Figure 10 illustrates the variation in the vertical displacement of the surrounding rock mass at different excavation stages. The roof of the excavated room initiated collapsing when the excavation length reached 8 m. The final maximum settlement of the roof was approximately 3 cm, while the maximum floor bulge was less than 1 cm. By the final stage, the sidewall remained stable, experiencing a maximum compression of less than 1 cm. In essence, noticeable deformation did not occur in the abandoned mining area throughout the excavation process, whether it was the roof or the floor. Moreover, horizontal displacement of the rock mass was less prominent than the vertical displacement, suggesting that both the roof and the sidewall were capable of maintaining stability in the excavation stage.

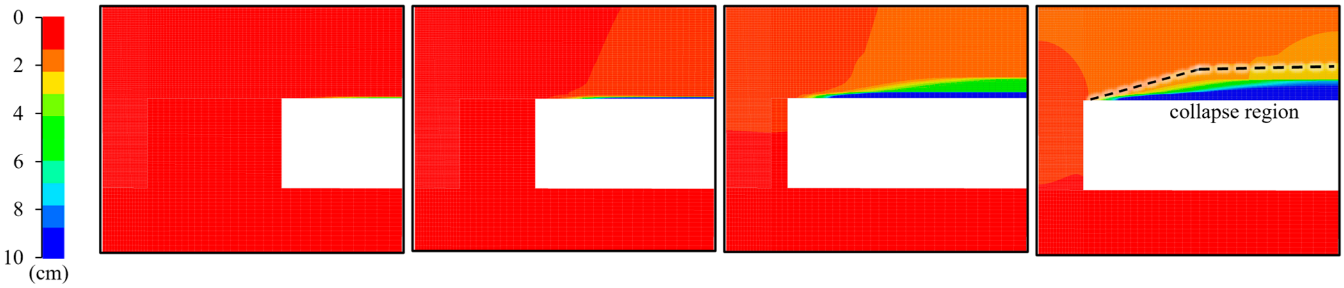

(**a**) 4 m (**b**) 6 m (**c**) 8 m (**d**) 8.5 m

Figure 10. Vertical displacement evolvement at different excavation states.

4.2. Medium- and Long-Term Stability Analysis

Based on the analyses in the last section, the numerical model of the abandoned mining area appears to remain stable during the excavation. However, some degree of damage did occur in the sidewall, leading to the formation of a relaxation region. This region may allow groundwater from upper layers to infiltrate the abandoned area through cracks and channels formed by the roof deformation. Over time, the relaxation region of the sidewalls will undergo softening and spalling, exposing the elastic core. This exposure will decrease the effective thickness and horizontal confining stress of the sidewall, leading to further damage and inevitably causing instability in the wall.

In light of this, a numerical model was established for further analysis, as depicted in Figure 11. Several assumptions were made for this model. The collapsed roof area shown in Figure 8 and the damaged sidewall area shown in Figure 9 have been completely destroyed, forming a 1 m thick collapsed mass at the bottom of the abandoned mining area. Due to sidewall damage and spalling, its thickness has decreased by 0.1 m compared with the initial model. The constitutive law of the collapsed mass follows the Mohr–Columb model, with detailed parameters listed in Table 2.

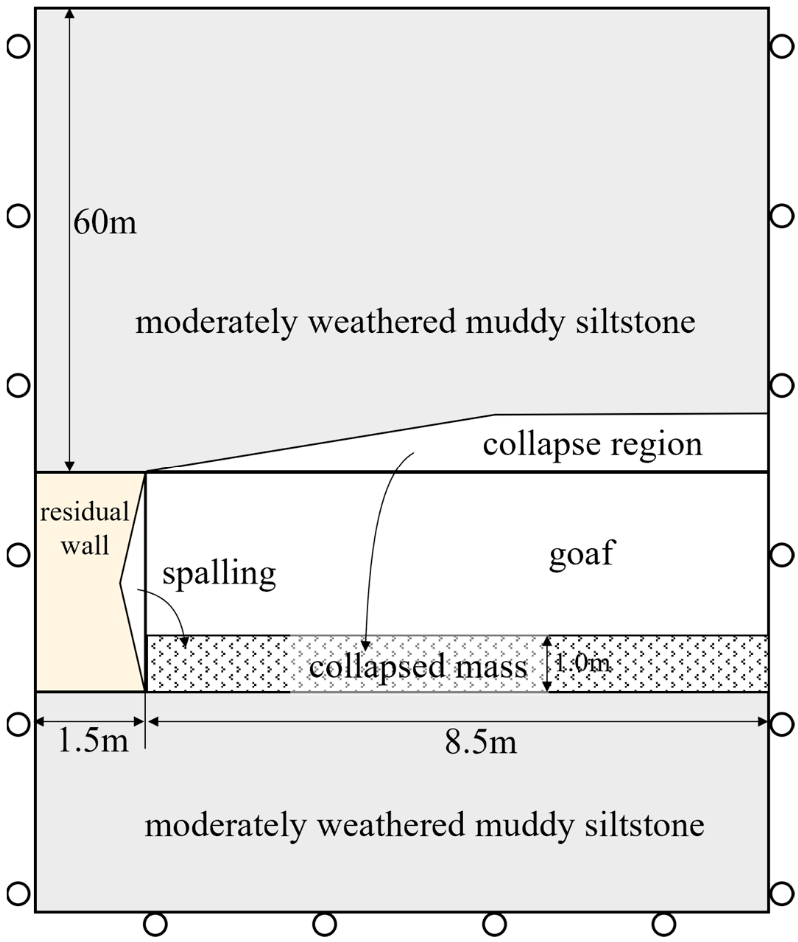

Figure 11. Numerical model setup for long-term stability.

Table 2. Numerical model parameters for collapsed mass.

	Density	Elastic Modulus	Poisson's Ratio	Cohesion	Friction Angle
	kg/m^3	GPa	/	kPa	°
Collapsed mass	2000	0.5	0.35	0	35

Figure 12 presents the vertical stress and displacement curves at the top of the sidewall, while Figure 13 illustrates the distribution of the vertical stress in the surrounding rock mas under varying spalling thicknesses of the sidewall. With increasing spalling collapse, the vertical stress at the monitoring point gradually rises. The stress curve peaks at a spalling thickness of 0.4 m, after which it starts to decline in conjunction with a continuous increase in vertical displacement. This trend suggests that the sidewall has become unstable. Regarding Figure 13, it indicates that as spalling intensifies, the elastic core experiences a significant increase in vertical stress. When the spalling thickness reaches 0.3 m, the elastic core is subjected to a vertical stress exceeding 20 MPa, which is close to the uniaxial compressive strength of gypsum rock in a laboratory (25 MPa). When the thickness reaches 0.4 m, the stress within the elastic core suddenly becomes disordered and then decreases, signaling a prelude to instability.

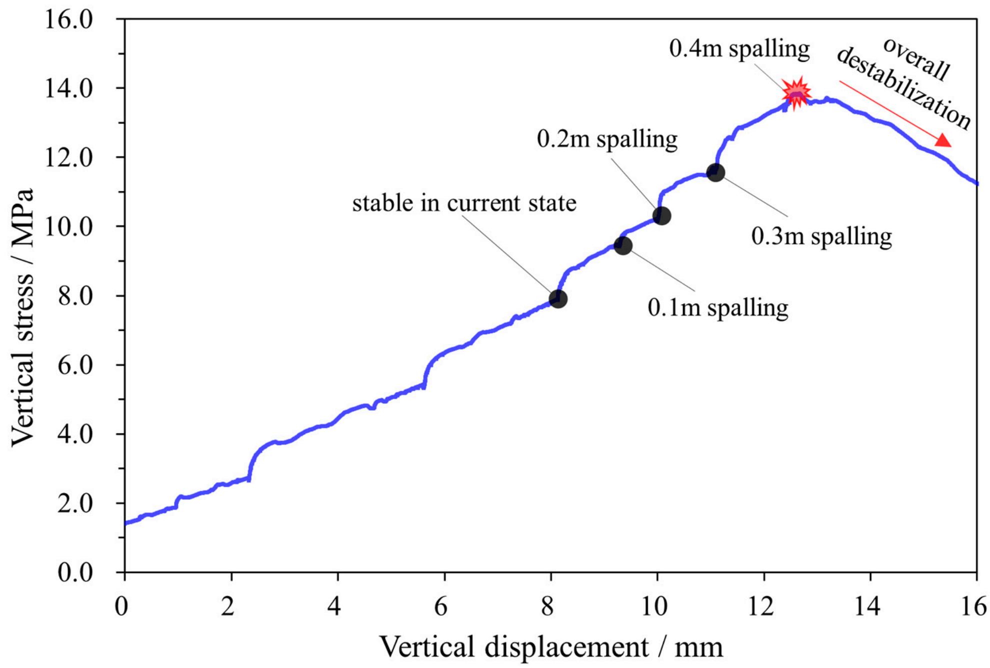

Figure 12. Vertical stress–vertical displacement curve at the monitoring point of long-term stability.

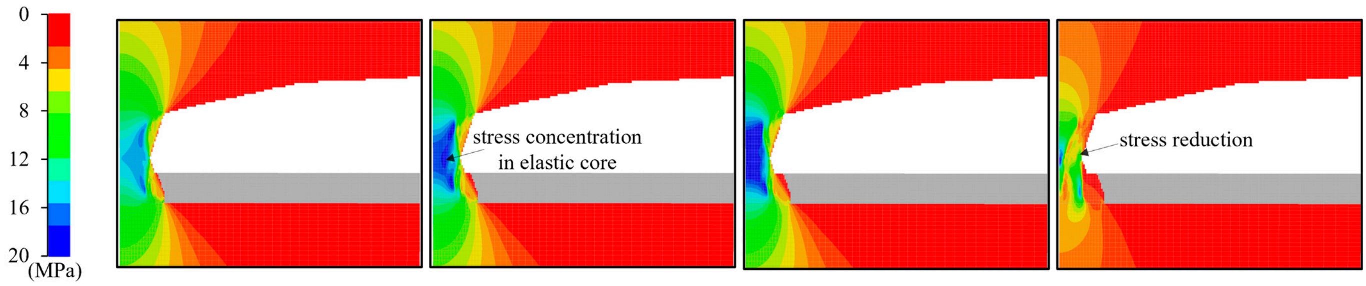

(**a**) 0.1 m (**b**) 0.2 m (**c**) 0.3 m (**d**) 0.4 m

Figure 13. Vertical stress evolvement at different wall damage states.

The evolution of the plastic elements (Figure 14) reveals that the tensile damage area at the top of the abandoned mining area remains relatively unchanged following the collapse of the roof. This lack of significant change can be attributed to the loss of tensile strength in the collapsed area during the previous excavation and the subsequent rebalancing of stress in the rock mass outside the collapsed roof region. Consequently, removing this region of rock mass is unlikely to substantially impact the plastic state of the model. In essence, the critical factor for the long-term stability of the abandoned mining area is the condition of the sidewall. Figure 14d illustrates that the shear plastic regions have become interconnected and cannot be constrained. Moreover, gypsum rock within the sustained plastic-yielding state exhibits a non-linear strain-softening behavior. After reaching the peak strength, it rapidly falls to the low residual strength.

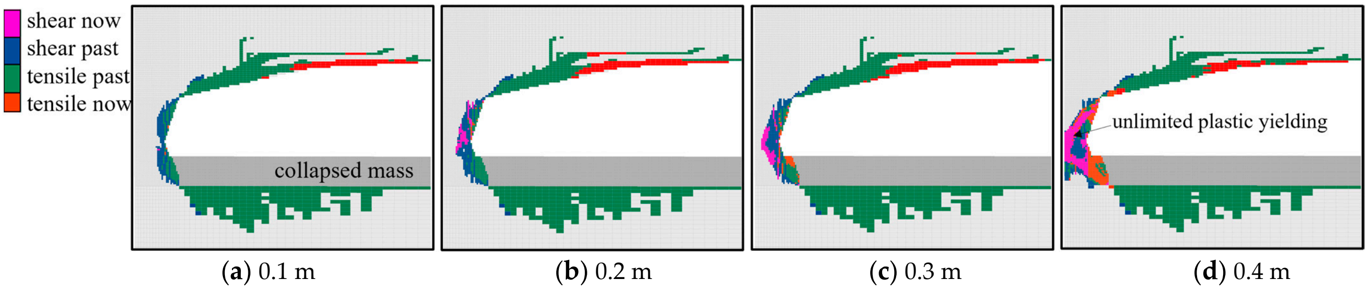

Figure 14. Plastic region evolvement at different wall damage states.

The sloss distribution index demonstrates that as the spalling of the sidewall expands, the gypsum rock continues to be damaged, with more elements gathering. This gathering signifies the collapsing mass and propagation of rock cracks. Ultimately, a macroscopic slip plane forms throughout the whole sidewall, leading to the overall instability in the abandoned mining area. In Figure 15, the area where the sloss index < 0 indicates a complete rock mass failure. Damage bands penetrate the entire width of the sidewall, and the elastic core is yielding. Consequently, the safety of the abandoned mining area is compromised due to the inadequate thickness of the sidewall. The instability of the sidewall will manifest once the spalling reduces its thickness to 0.4 m. Without the implementation of protective treatment, this outcome is inevitable. Thus, it can be concluded that the long-term stability of the abandoned mining area cannot be ensured.

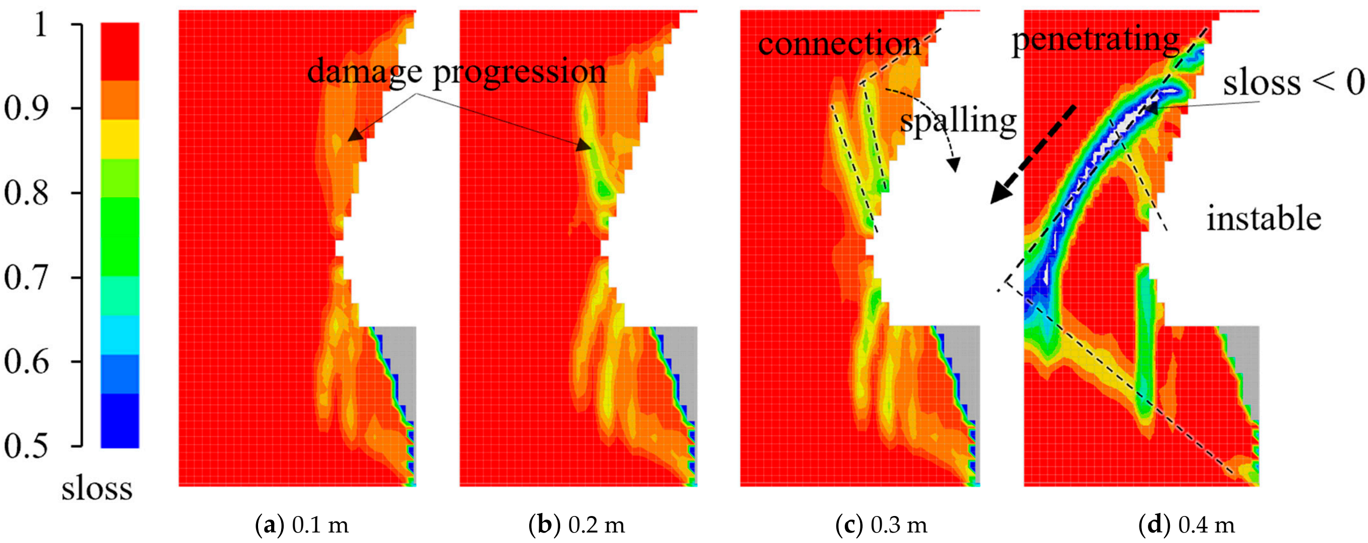

Figure 15. Sloss evolvement at different wall damage states.

4.3. Filling Treatment Effect

As discussed earlier, the long-term stability of the sidewall cannot be ensured. Therefore, implementing a protective treatment is crucial to maintaining the integrity of the abandoned mining area. The application of mortar filling is a viable approach in this context. This method can effectively reduce deformation and improve the stress distribution and the overall stability of the rock mass. Figure 16 illustrates the corresponding numerical model used to assess the impact of the mortar filling method under various conditions, with a spalling thickness of 0.4 m. The constitutive relationship of the mortar adheres to the Mohr–Columb model, and specific parameters are detailed in Table 3.

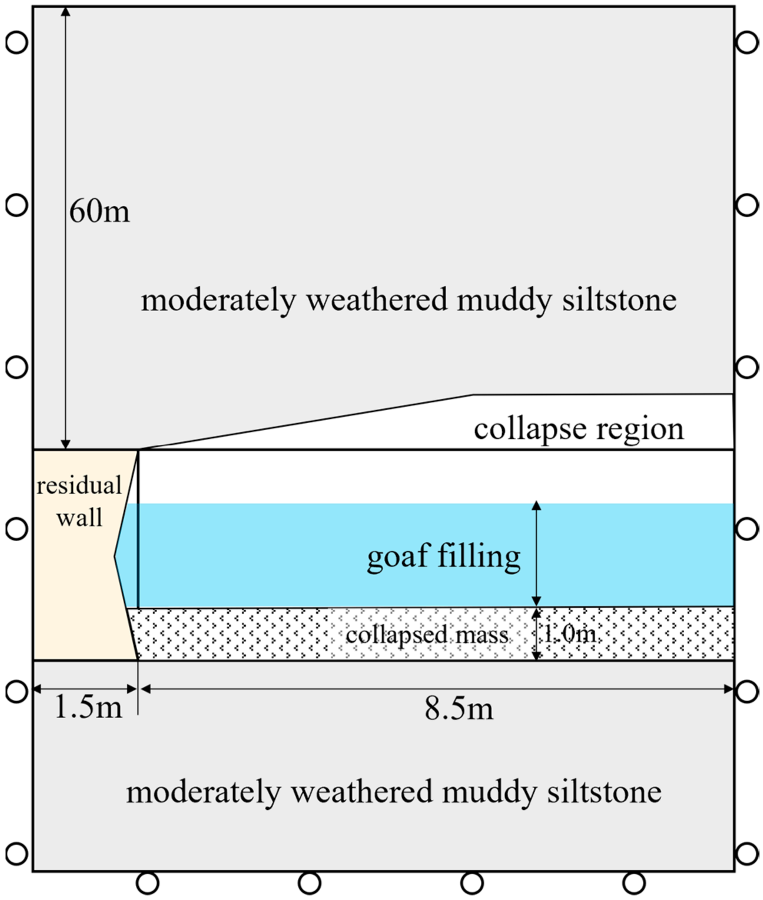

Figure 16. Numerical model setup for filling states.

Table 3. Numerical model parameters for filling materials.

	Density	Elastic Modulus	Poisson's Ratio	Cohesion	Friction Angle
	kg/m^3	GPa	/	kPa	°
Filling	2200	1	0.25	1	35

The vertical stress and displacement curves at the top of the sidewall are presented in Figure 17, while Figure 18 depicts the vertical stress distribution in the surrounding rock mass under different conditions. The reinforcement provided by the mortar filling prevents a stress drop within the core compression region of the sidewall, as seen in Figure 18d, resulting in a final stress interval ranging from 16 to 20 MPa. Nevertheless, Figure 19 reveals that interconnected plastic zones still emerge when the mortar's height is below half of the sidewall's height. However, the plastic elements are constrained once the mortar's height exceeds this threshold.

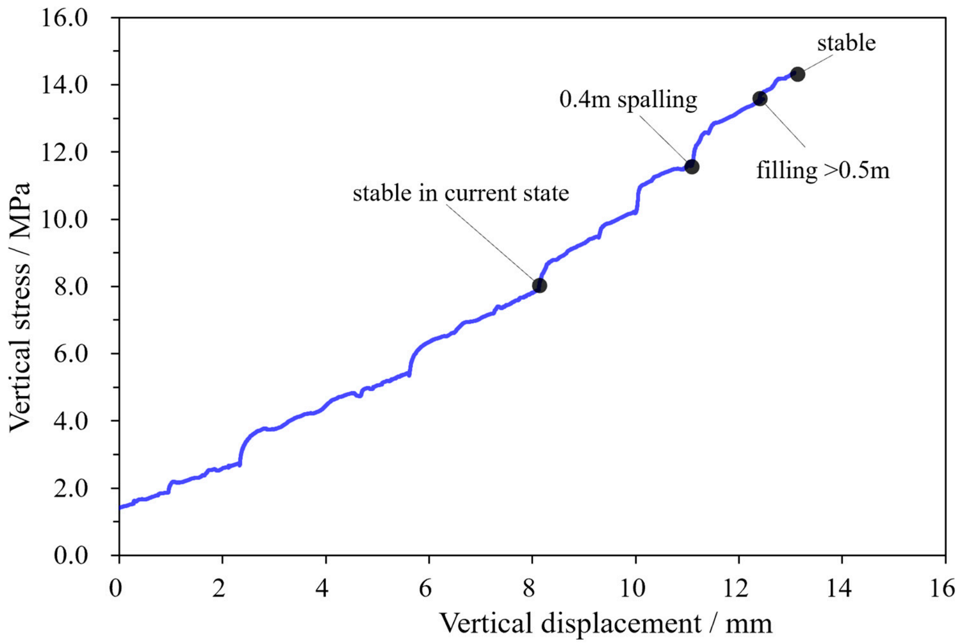

Figure 17. Vertical stress–vertical displacement curve at the monitoring point after filling.

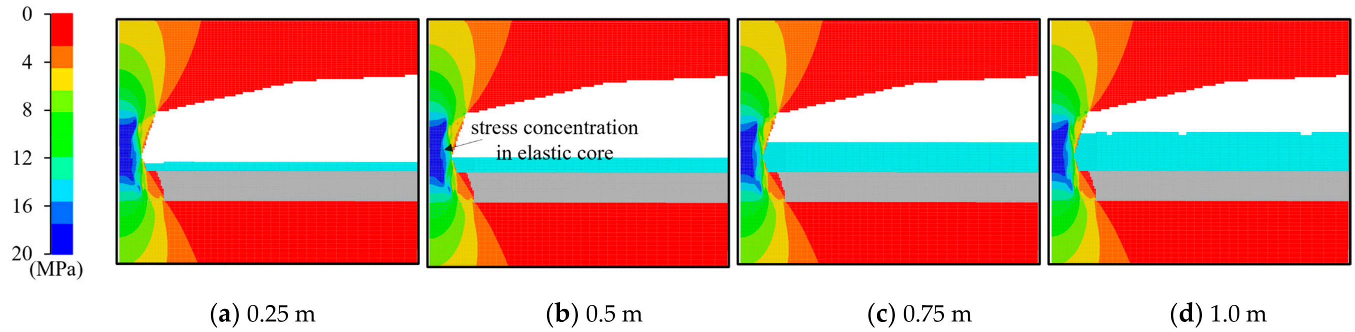

Figure 18. Vertical stress evolvement at different filling heights.

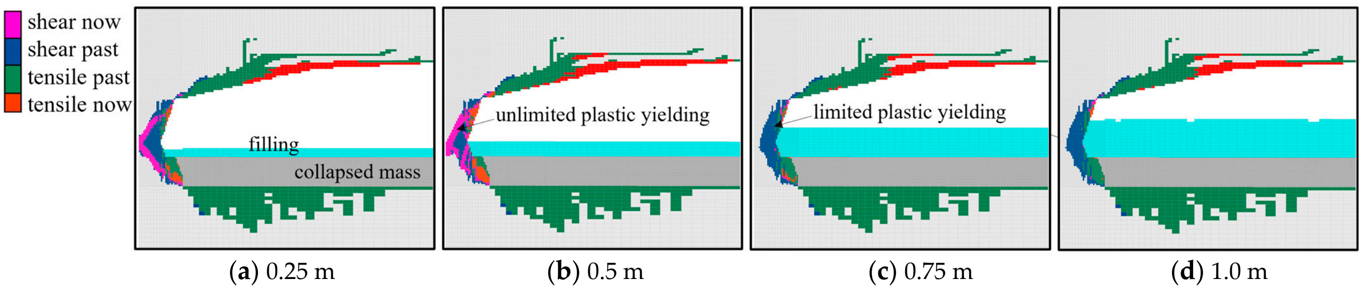

Figure 19. Plastic region evolvement at different filling heights.

Figure 20 shows that an inadequate mortar filling height leads to significant damage development in the rock mass at the upper area of the sidewall, with a tendency towards deeper faulting. Conversely, a sufficient filling height restricts further damage progression in the sidewall's rock mass and prevents surface softening and spalling due to groundwater seepage. Figure 20d indicates the formation of a 5 MPa principal stress within the filled mortar near the sidewall, signifying that the filler can share the load carried by the sidewall. As a result, the mortar filling substantially enhances the lateral support of the sidewall, improves the stress distribution in the damaged rock mass, and prevents sidewall instability.

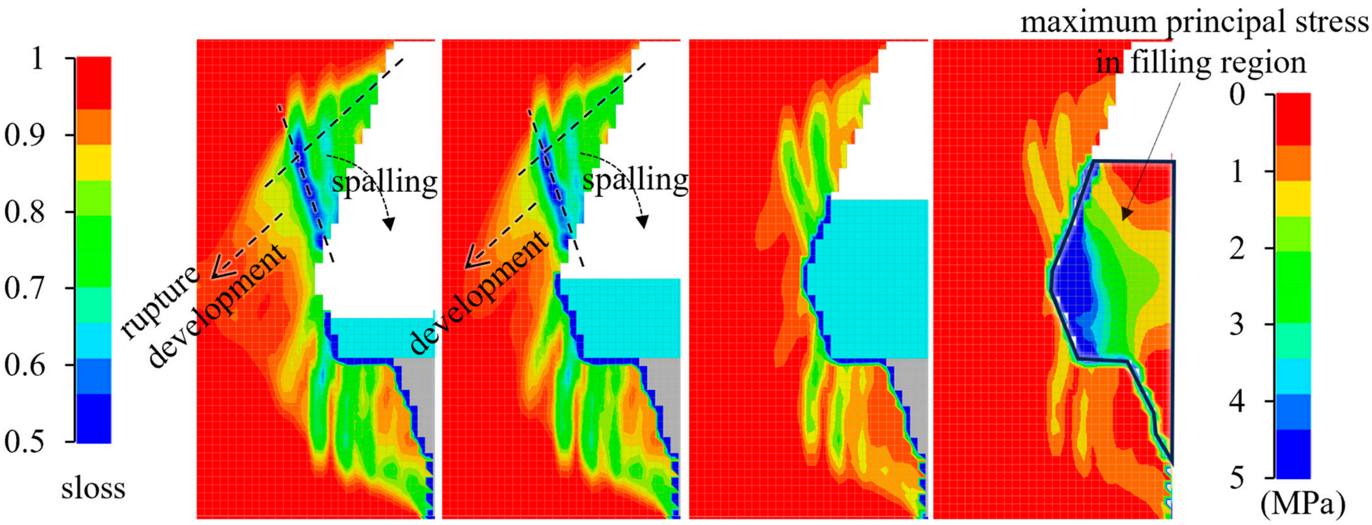

(**a**) 0.25 m (**b**) 0.5 m (**c**) 0.75 m (**d**) 1.0 m

Figure 20. Sloss evolvement at different filling heights.

5. Conclusions

This paper used the laser scanning method through boreholes to obtain three-dimensional point cloud data of an abandoned gypsum mine in south China. It reconstructed the three-dimensional spatial morphology of the actual gypsum mining rooms beneath the transportation infrastructure and established a numerical stability analysis model for the abandoned gypsum mine from mining excavation to long-term stages using the IMASS rock mass constitutive model. The following main conclusions are drawn:

(a) The IMASS rock mass constitutive model can effectively reflect the entire process of rock mass from microscopic damage to macroscopic instability, and the numerical simulation of current and long-term stages provides a much greater understanding of the mining room stability and the effect of various geo-mechanical parameters not considered in traditional empirical methods.

(b) Through the proposed numerical analysis, it is revealed that the stability of the roof in the medium-weathered rock layer is relatively assured, and the stability of the abandoned gypsum mine is mainly controlled by the residual sidewalls. In the current stage, the abandoned gypsum mine stability is guaranteed. The numerical results show that a 0.4 m spalling can cause the overall instability and failure of the sidewall. This is almost inevitable in the medium to long term as the gypsum rock mass continues to soften and deteriorate. Therefore, reinforcement measures must be taken to ensure safety.

(c) Using numerical simulation methods, the stability of the abandoned gypsum mine with filling solutions was evaluated. Assuming the residual collapsed mass and the filling cement body reach a height of 2 m, the stress state of the sidewall is effectively improved. Of course, the higher the filling rate, the more it can prevent sidewall softening and spalling, especially due to the groundwater influence.

Author Contributions: Conceptualization, Y.S.; investigation, H.W. and Y.J.; supervision, X.T.; writing—review and editing, X.T.; visualization, J.W.; software, B.T. All authors have read and agreed to the published version of the manuscript.

Funding: This study was funded by the "National Natural Science Foundation of China (52278348)" and the "Transportation Science and Technology Development and Innovation Project of Hunan Province (202303-2)".

Institutional Review Board Statement: Not applicable.

Informed Consent Statement: Not applicable.

Data Availability Statement: Data are contained within the article.

Conflicts of Interest: Author Yungang Shi, Yuxuan Jin, and Bigang Tang are employed by the Hunan Communications Research Institute Co., Ltd. Author Huaijian Wang is employed by the CCCC Construction Group Co., Ltd. The remaining authors declare that the research was conducted in the absence of any commercial or financial relationships that could be construed as a potential conflict of interest.

References

1. Sadeghiamirshahidi, M.; Vitton, S.J. Laboratory Study of Gypsum Dissolution Rates for an Abandoned Underground Mine. *Rock Mech. Rock Eng.* **2019**, *52*, 2053–2066. [CrossRef]
2. Du, X.-H.; Li, X.; Feng, Q.; Meng, L.; Sun, Y. Environmental risk assessment of industrial byproduct gypsum utilized for flling abandoned mines. *Int. J. Coal Sci. Technol.* **2022**, *9*, 214–225. [CrossRef]
3. Xu, X.; Cui, X.; Liu, X.; Tang, Q.; Zhang, X.; Sun, Y.J.G. Damage analysis of soaking gypsum and safety evaluation of goaf: Based on energy dissipation theory. *Geotech. Geol. Eng.* **2020**, *38*, 6177–6188. [CrossRef]
4. Xu, Z.; Xu, W.; Zhu, Z.; Zhao, J. Research on monitoring and stability evaluation of ground subsidence in gypsum mine goaf. *Front. Environ. Sci.* **2023**, *10*, 1097874. [CrossRef]
5. Yang, Y.; Xing, L.-Y.; Zhang, Y.-Q.; Ma, D. Analysis of long-term stability of gypsum pillars based on creep tests. *Chin. J. Rock Mech. Eng.* **2015**, *34*, 2106–2113.
6. Xia, K.; Chen, C.-X.; Liu, X.-M.; Zhou, Y.; Jiang, X. Study of the failure of pillar-roof system in gypsum mines based on catastrophe theory. *Chin. J. Rock Mech. Eng.* **2016**, *35*, 3837–3845.
7. Xu, X.-D.; Zhou, Y.-J.; Pang, S. Analysis of catastrophic instability of plastic supporting system in old goaf of gypsum mine. *Chin. J. Rock Mech. Eng.* **2018**, *37*, 2548–2555.
8. Henley, S. Catastrophe theory models in geology. *Math. Geol.* **1976**, *8*, 649–655. [CrossRef]
9. Auvray, C.; Homand, F.; Hoxha, D. The influence of relative humidity on the rate of convergence in an underground gypsum mine. *Int. J. Rock Mech. Min. Sci.* **2008**, *45*, 1454–1468. [CrossRef]
10. Auvray, C.; Homand, F.; Sorgi, C. The aging of gypsum in underground mines. *Eng. Geol.* **2004**, *74*, 183–196. [CrossRef]
11. Zhao, Y.-L.; Wu, Q.-H.; Wang, W.-J.; Wan, W.; Zhao, F.J. Strength reduction method to study stability of goaf overlapping roof based on catastrophe theory. *Chin. J. Rock Mech.* **2010**, *29*, 1424–1434.
12. Pierce, M.; Cundall, P. Numerical simulations of block caving induced surface subsidence. *Int. J. Rock Mech. Min. Sci.* **2004**, *41*, 423–431.
13. Cai, M.; Kaiser, P.K.; Uno, H.; Tasaka, Y.; Minami, M. Estimation of rock mass deformation modulus and strength of jointed hard rock masses using the GSI system. *Int. J. Rock Mech. Min. Sci.* **2007**, *44*, 247–265. [CrossRef]
14. Alejano, L.R.; Gomez, R. A method for assessing the stability of tunnels in blocky rock. *Tunn. Undergr. Space Technol.* **2013**, *36*, 37–49.
15. Fidelibus, C.; Soccodato, F. Numerical analysis of stability and collapse mechanisms of underground limestone quarries in Apulia, Italy. *Eng. Geol.* **2002**, *66*, 249–264.
16. Zou, Y.; Konietzky, H. Numerical simulation of water inflow from an underlying karstic aquifer into an underground mine. *Environ. Earth Sci.* **2016**, *75*, 1–15.
17. Ghazvinian, E.; Fuenzalida, M.; Orrego, C.; Pierce, M. Back analysis of cave propagation and subsidence at Cadia EastMine. In Proceedings of the Eighth International Conference & Exhibition on Mass Mining, Santiago, Chile, 9–11 December 2020.
18. Hoek, E.; Diederichs, M.S. Empirical Estimation of Rock Mass Modulus. *Int. J. Rock Mech. Min. Sci.* **2006**, *43*, 203–215. [CrossRef]
19. Hoek, E.; Carranza-Torres, C.; Corkum, B. Hoek-Brown Failure Criterion—2002 Edition. In *NARMS-TAC 2002: Mining and Tunnelling Innovation and Opportunity*; Hammah, R., Bawden, W., Curran, J., Telesnicki, M., Eds.; University of Toronto Press: Toronto, ON, Canada, 2002; Volume 1, pp. 267–273.
20. Alejano, L.R.; Alonso, E. Considerations of the dilatancy angle in rocks and rock masses. *Int. J. Rock Mech. Min. Sci.* **2005**, *42*, 481–507. [CrossRef]